applied sciences

MDPI

Article

Simultaneous PAN Carbonization and Ceramic Sintering for Fabricating Carbon Fiber-Ceramic Composite Heaters

Daiqi Li [1,2], Bin Tang [1,2], Xi Lu [1], Quanxiang Li [1], Wu Chen [2], Xiongwei Dong [2], Jinfeng Wang [1,2,*] and Xungai Wang [1,2,*]

1 Deakin University, Institute for Frontier Materials, Geelong/Melbourne, Victoria 3216, Australia; lidaiq@deakin.edu.au (D.L.); bin.tang@deakin.edu.au (B.T.); Lahshiy@outlook.com (X.L.); quanxiang.li@deakin.edu.au (Q.L.)

2 Wuhan Textile University, Joint Laboratory for Advanced Textile Processing and Clean Production, Wuhan 430073, China; wuchen@wtu.edu.cn (W.C.); xwdong@wtu.edu.cn (X.D.)

* Correspondence: xungai.wang@deakin.edu.au (X.W.); jinfeng.wang@deakin.edu.au (J.W.); Tel.: +61-3-5227-2012 (J.W.)

Received: 15 October 2019; Accepted: 14 November 2019; Published: 17 November 2019



Abstract: In this study, a single firing was used to convert stabilized polyacrylonitrile (PAN) fibers and ceramic forming materials (kaolin, feldspar, and quartz) into carbon fiber/ceramic composites. For the first time, PAN carbonization and ceramic sintering were achieved simultaneously in one thermal cycle and the microscopic morphologies and physical features of the obtained carbon fiber/ceramic composites were characterized in detail. The obtained carbon fiber/ceramic composite showed comparable flexural strength as commercial ceramic tiles. Meanwhile, the composite showed exceptional electro-thermal performance based on the electro-thermal performance of the carbonized PAN fibers, which could reach 108 °C after 15 s, 204 °C after 90 s, and 292 °C after 450 s at 5 V (2.6 A), thereby making the ceramic composite a good candidate as an indoor climate control heater, defogger device, kettle, and other heating element.

Keywords: one-step firing method; PAN carbonization; ceramic; composite; electro-thermal performance

1. Introduction

Electricity driven resistive heaters have been widely used in energy conversion [1–3]. As current passes through the conductive materials, inelastic collisions between accelerated electrons and phonons occur and generate heat under an applied voltage [4]. Metallic materials (e.g., copper and silver) have been commonly used as heating elements [5]. However, these heating elements have relatively high density and rigidity. Recent research has focused on using carbonaceous materials as heating elements including carbon nanotubes (CNTs), graphene, and carbon fiber [2,6]. However, the agglomeration issues and difficulty of dispersing of CNT/graphene could lead to higher costs and time consumption during the manufacturing process. [7] Compared with other heating elements, carbon fiber is a flexible conducting material with low density and high strength [5]. Carbonaceous electrical heaters are now used in wearable heating fabric, heating equipment, defogger devices, and thermal therapy [1,4,8]. However, very few carbonaceous electrical heaters are used in floor or wall tiles for indoor climate control, which requires reliable mechanical properties, high thermal conductivity, and safe insulation of the surface parts.

Ceramic is an ideal material as the surface element of electrical heaters because of its particular advantages such as low density when compared to metal, excellent chemical inertness, high thermal conductivity, reliable mechanical property, good insulation, and low cost [9]. The triaxial

kaolin–feldspar–quartz is one of the most commonly used ceramic systems and widely used as earthenware, stoneware, domestic porcelain, dental porcelain, and insulators [10,11]. The obtained final phase of ceramic is mullite, which is an excellent thermal conductive material [12]. Many researchers have studied the interface between the fiber and ceramic matrix to achieve functional ceramic composites for electromagnetic shielding applications [13–16]. However, little has been reported on applying ceramics as electricity driven resistive heaters [17–19].

In a typical fabrication process of the carbon fiber/ceramic composites, carbon fiber is produced first and then fired together with ceramic precursors in the subsequent firing process. Therefore, two firing steps were needed to produce the carbon fiber/ceramic composites. It would save significant energy and time if the carbon fiber precursor and ceramic precursor can be fired together through a single firing to obtain the carbon fiber/ceramic composites. The most commonly used precursor for carbon fiber is polyacrylonitrile (PAN) [20]. PAN fibers are strong and flexible, and can be more easily handled than the relatively brittle carbon fibers [21].

Herein, we report a novel method to achieve the fabrication of carbon fiber/ceramic composites from the mixture of carbon fiber precursor PAN and ceramic precursor through a single firing process. During the firing process, the PAN carbonization and ceramic sintering were accomplished simultaneously. The mechanical properties of the carbon fiber/ceramic composite were examined. The microscopic morphologies and physical features including linear shrinkage, weight loss, bulk density, open porosity, and water absorption were characterized. The firing temperature effect on the composite performance was also investigated. Furthermore, the electro-thermal performance of the as-prepared composite was analyzed. The as-prepared carbon fiber/ceramic composite showed great potential to be used as indoor climate control heaters.

2. Materials and Methods

2.1. Materials

Kaolin and quartz were purchased from Chem-Supply Pty. Ltd., Australia. Feldspar was supplied by Lingshou Shikuang Company, China. PAN precursor tow (12K) was obtained from Jilin Chemical Fiber Co. Ltd., China.

2.2. Composite Fabrication

Kaolin, feldspar, and quartz powders were dried in an oven at 80 °C for 10 h. Then kaolin, feldspar, and quartz with a typical ratio of 2:1:1 were mixed through a TURBULA®T2F Mixer [22]. The mixed powder was moistened by spraying with ethanol (6 wt.%). The powder (~12 g) was then poured into a 50 × 50 mm steel die as a bottom layer. PAN fibers were put into a furnace under 238 °C for 20 min, 248 °C for 20 min, and then 260 °C for 20 min for pre-oxidation or stabilization treatment. Then, two bundles of stabilized PAN fibers (0.21 g) were laid separately in the die. Subsequently, a top layer of mixed powder (~12 g) was added into the die. The die was subjected to a pressure of 30 MPa and maintained at this pressure for 5 min. The obtained green body with 1.7 wt.% of PAN fibers was dried in an oven at 80 °C for 10 h and then subjected to sintering in a tube furnace at a certain temperature with a heating rate of 10 °C/min in a nitrogen atmosphere. The green body was maintained at the highest temperature for 1 min and then cooled down to room temperature naturally. Four different sintering temperatures were determined according to the ceramic manufacture process, [23–25] which were 1200 °C, 1250 °C, 1300 °C, and 1350 °C. The obtained samples were denoted as Composite-1200, Composite-1250, Composite-1300, and Composite-1350, respectively. The manufacture process is illustrated in Figure 1.

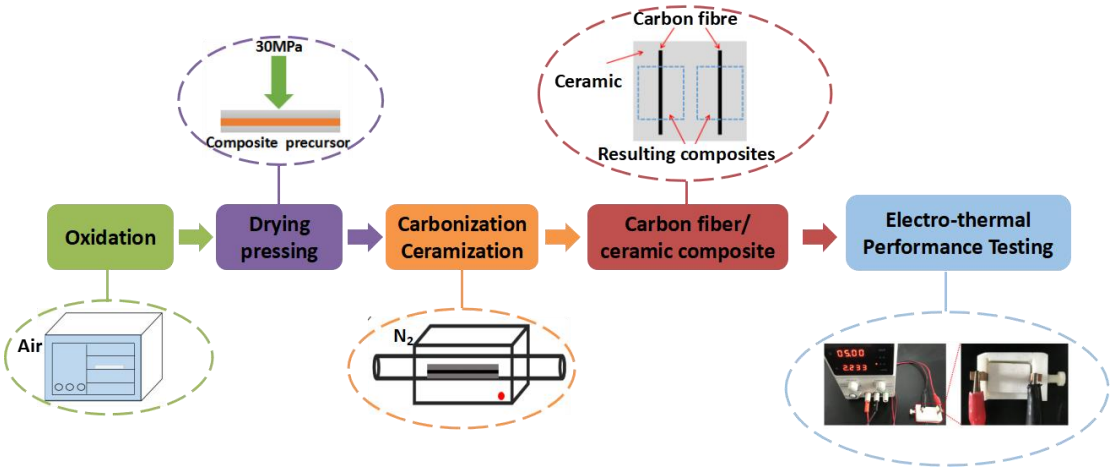


Figure 1. Scheme of the fabrication process of the ceramic composite with carbon fiber.

For comparison, 25 g mixed ceramic powder without pre-oxidized PAN was added into the die and subjected to 30 MPa, which was then fired under the same conditions as the carbon fiber/ceramic composite at 1200 °C, 1250 °C, 1300 °C, and 1350 °C. The prepared samples were denoted as Ceramic-1200, Ceramic-1250, Ceramic-1300, and Ceramic-1350, respectively.

2.3. Characterization

The particle sizes of kaolin, feldspar, and quartz were measured using a Malvern Mastersizer 2000. The loss on ignition, LOI (%), of the fired samples was calculated via the following equation, [26]

$$\mathrm{LOI}\% = \frac{W_D - W_I}{\mathrm{W}_D} \times 100 \quad (1)$$

where W_D is the weight of the green body and W_I is the weight of the ceramic after the firing process. The sample linear shrinkage in length (Ls) was calculated as Equation (2) [24]

$$\mathrm{Ls} = \frac{L_0 - L}{L_0} \times 100 \quad (2)$$

where L_0 is the length of the green body and L is the length of the ceramic after the firing process.

The bulk density, water absorption, open porosity, and bending strength properties were measured according to EN ISO 10545. [27] Briefly, the dry mass (D) of the sample was measured first. Then, the sample was immersed into boiling deionized water for 5 h and soaked for 24 h at ambient temperature, then mass (S) of the sample suspended by fine wire in water, and the water-saturated mass (W) was weighed. The total volume (V) of the sample can be measured by V = W − S.

Bulk density (B) can be calculated via Equation (3).

$$\mathrm{B} = \frac{D}{\mathrm{V}} \quad (3)$$

Water absorption (WA) (%) is calculated via Equation (4).

$$\mathrm{WA}\% = \frac{W - D}{\mathrm{D}} \times 100 \quad (4)$$

The open porosity, ε (%) can be described as Equation (5).

$$\varepsilon\% = \frac{W - D}{\mathrm{V}} \times 100 \quad (5)$$

The specimens were then cut into a size of 30 × 20 mm with the thickness of 4.5 mm by a Struers Accuton-100 cut-off machine for mechanical and electrothermal performance tests. A three point flexural test was used to measure the mechanical properties of the obtained composite samples. This flexural strength test was carried out using an Instron 5567 universal testing machine with a span of 20 mm and a cross head speed of 0.5 mm/min. L represents the support span (mm); b represents the width of test samples (mm); d is the thickness of the tested sample (mm); and F is the load at a given point on the load deflection curve (N). The bending strength σ_f is calculated via Equation (6). [27]

$$\sigma_f = \frac{3FL}{2bd^2} \tag{6}$$

The samples were fractured in liquid nitrogen and the scanning electron microscopy (SEM) images of the fracture surface was then obtained by scanning electron microscope (LEO SEM S440 from Carl Zeiss, Germany). The powder x-ray diffraction (XRD) patterns of the samples were collected by an x-ray diffractometer (Analytical/X'Pert Powder) using Cu Kα radiation (λ~1.54 Å) over a range of 5 to 70° (2θ) at a rate of 2.4 °/min. The carbonization degree of carbon fiber was characterized by Raman spectrometer (Renishaw inVia Raman Microscope) at a laser wavelength of 514 nm. The spectra were collected at 10% of the nominal power (50 mW) for 10 s. The carbon fibers were extracted from the composites and washed for 30 min by sonication before characterization. The obtained carbon fibers were denoted as CF-1200, CF-1250, CF-1300, and CF-1350. For comparison, the pre-oxidized PAN fibers were put into the furnace without ceramic precursor and fired at 1200 °C, which was named as PAN-1200.

The electrical resistance of the as-prepared samples were measured by a multimeter (FLUKE 189). Infrared thermal imaging technology was used to characterize the electro-thermal performance. The composites were connected to a power supply (KORAD, KD3005D) at 2 V to 5 V and the joule heating performance was recorded by a thermal camera (FLIR ONE PRO).

3. Results and Discussion

3.1. Component Analysis

The average particle sizes of the raw materials of kaolin, feldspar, and quartz were measured as 6.1, 122.5, and 6.8 μm, respectively. Figure 2a shows the XRD patterns of the raw materials and specimens fired at different temperatures from 1200 °C to 1350 °C. The major phases of kaolin, feldspar, and quartz can be observed clearly in the XRD patterns of the precursor materials [28]. During the firing process, kaolin transforms to metakaolin at around 980 °C and the metakaolin transforms to mullite at around 1100 °C [25,29]. Meanwhile, feldspar starts to melt at temperatures above 1100 °C [22]. The feldspar disappeared in all of the fired ceramic composites with fibers. Mullite and quartz were the major crystalline phases observed in the final composites fired at different temperatures from 1200 °C to 1350 °C [30]. The conclusions from the XRD characterization in the present study is consistent with that from the thermogravimetric analysis (TGA) data in a previous report [31].

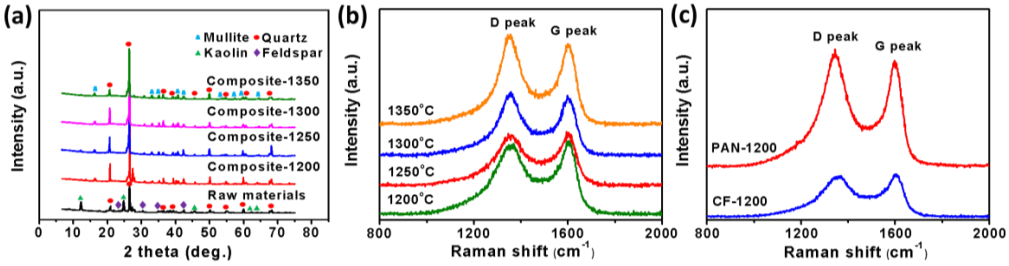


Figure 2. (**a**) X-ray diffraction (XRD) patterns of the raw materials and the obtained specimens fired at different temperatures, (**b**) Raman spectra of the carbon fibers sintering at different temperatures and **(c)** carbonization in and outside the ceramic.

Raman scattering spectroscopy was used to investigate the carbonization degree of PAN during the one step firing process. Figure 2b,c show the Raman scattering spectra of the carbon fibers from different composites. Two peaks at 1350 cm^{-1} and 1590 cm^{-1}, attributed to the D peak and G peak of carbon materials, were observed for all fibers fired at the four different temperatures, which demonstrates the successful carbonization of precursor PAN fibers. The D peak at 1350 cm^{-1} can be attributed to the disordered and defect carbonaceous structure. The G peak at 1590 cm^{-1} represents the ordered graphitic structure [32,33]. R value as the intensity ratio of D peak (I_D) and G peak (I_G) is used to analyze the graphitization degree of carbon fiber. As the temperature increased from 1200 °C to 1350 °C, the R value increased from 0.94 to 1.15 (Figure 2b), which is typical of the onset of a carbonized structure [34]. R values of CF-1200 (extracted from Composite-1200) and PAN-1200 (PAN fiber directly carbonized without ceramic precursor, tension, and compression) were 0.94 and 1.10, respectively (Figure 3c). This implies that the ceramic precursor environment and the compression facilitate the formation of highly ordered carbonaceous structure.

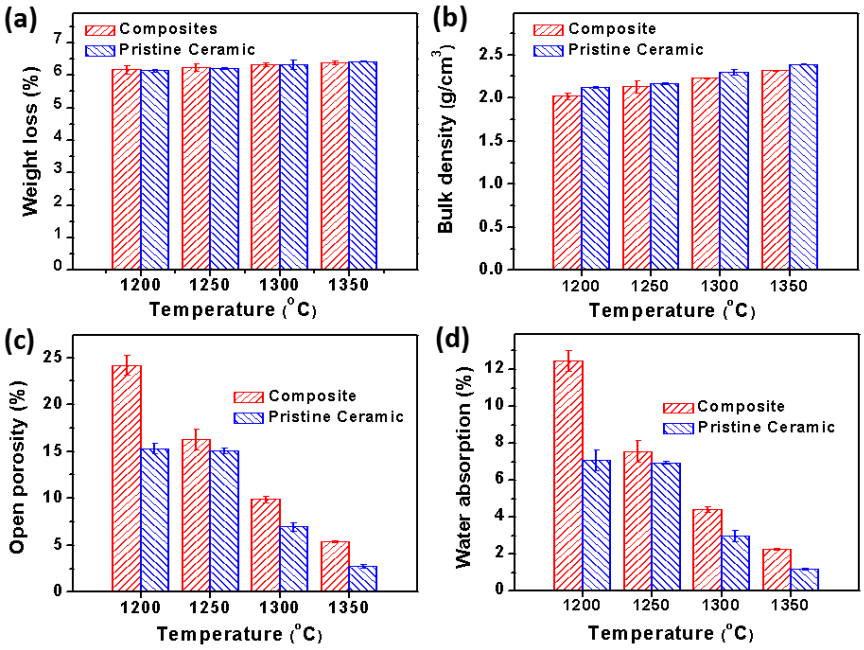


Figure 3. Physical properties of composites fired at different temperatures. (**a**) Weight loss, (**b**) bulk density, (**c**) open porosity, and (**d**) water absorption.

3.2. Physical Parameters of the Composites

Ceramic composites showed a similar weight loss and bulk density as pristine ceramic (Figure 3a,b). No obvious difference in weight loss was observed when the firing temperature was increased from 1200 °C to 1350 °C (Figure 3a), which indicates that the weight loss mainly occurred at a temperature lower than 1200 °C. The main weight loss came from the dihydroxylation of kaolin as shown as follows [24,29,35].

$$2SiO_2 \cdot Al_2O_3 \cdot 2H_2O \text{ (Kaolin)} \rightarrow 2SiO_2 \cdot Al_2O_3 \text{ (Metakaolin)} + 2H_2O \quad (7)$$

Meanwhile, the bulk density of the composites increased slightly from 2.02 g/cm^3 for Composite-1200 to 2.32 g/cm^3 for Composite-1350 (Figure 3b). This increase may be attributed to the reduced volume from the shrinkage of the specimen.

The open porosity of the composites reduced greatly from 24.19% for Composite-1200 to 5.39% for Composite-1350 (Figure 3c). The porosity between carbon fiber and ceramic, together with the un-densification of the ceramic, are the two main reasons for the formation of the open porosity. As the temperature increased, feldspar started to melt, and transformed to a glassy phase around 1100 °C,

which enabled it to permeate into the microstructure, leading to the decreased open porosity [22,24]. Water absorption is related to open porosity, as shown in Figure 3d. Water absorption of the ceramic composites decreased from 12.45% to 2.29% as the firing temperature was increased from 1200 °C to 1350 °C. The open porosity of pristine ceramic reduced from 15.3% to 2.75% after sintering from 1200 °C to 1350 °C. Meanwhile, the water absorption of pristine ceramic also decreased from 7.1% to 1.2%. The reduction in open porosity and water absorption of the composites is attributed to the densification of the ceramic. Whereas, compared with pristine ceramic, the composites exhibited increased open porosity and higher water absorption, which is due to the presence of a gap between the ceramic and carbon fibers in the composites. Work is on-going to optimize the mechanical properties of the carbon fiber/ceramic composites.

The obtained carbon fiber/ceramic composites were white in color after sintering, as shown in Figure 4a. The sintering process led to shrinkage of the composites and the linear shrinkage of the composites increased with an increase in the firing temperature (Figure 4b). The linear shrinkage values were 2.23% for Composite-1200 and 6.97% for Composite-1350. The linear shrinkage of all of the composites showed the same trend as that of pristine ceramic.

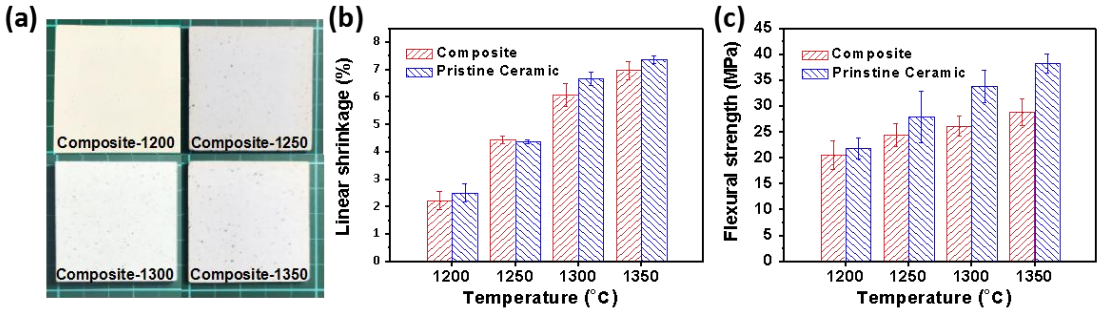


Figure 4. (**a**) Optical pictures, (**b**) linear shrinkage, and (**c**) flexural strength of specimens fired at different temperatures.

A three point flexural test was carried out to evaluate the flexural strength of the obtained carbon fiber/ceramic composites. Figure 4c shows the flexural strength of the carbon/fiber composites and pristine ceramic, which were prepared at different temperatures. The flexural strength of both the ceramic composites and pristine ceramic increased as the firing temperature increased, which may be caused by the reduced porosity (Figure 3c). The flexural strength of the ceramic composite reached 28.88 MPa at 1350 °C. Compared with the ceramic composites, the pristine ceramic without carbon fibers showed a higher flexural strength of 38.25 MPa at 1350 °C. It is suggested that the gaps between the carbon fiber and ceramic resulted in the lower flexural strength of the ceramic composite.

3.3. Micromorphology of the Composites

The scanning electron microscope (SEM) images of the ceramic composite cross-sections are displayed in Figure 5. It can be seen that the fibers were pulled-out during the cracking, which indicates that there was a weak fiber/ceramic interfacial bonding. Figure 5a–c show that two different layers of carbon fibers co-existed in the composites. In the outer layer, the ceramic infiltrated into the carbon fibers, while the carbon fibers in the inside layer showed a much longer pull-out fiber length than that of the outer carbon fiber, which may be caused by the ceramic not infiltrating into the inside of the fiber bundles. Composite-1300 showed a reduced fiber pull-out length than Composite-1200. This may be attributed to the higher density of Composite-1300 and the increased density may improve the interaction between the carbon fibers and ceramic, leading to reduced fiber pull-out length.

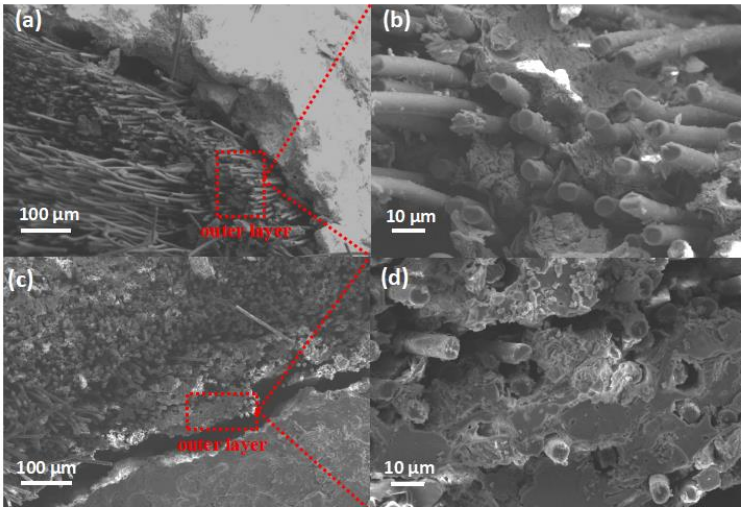


Figure 5. Scanning electron microscope (SEM) images of the specimen cross sections fired at (**a**,**b**) 1200 °C and (**c**,**d**) 1300 °C.

3.4. Evaluation of Electro-Thermal Performance

Figure 6a shows the resistance of the carbon fibers decreased from 2.4 Ω to 1.9 Ω as the sintering temperature increased from 1200 °C to 1350 °C. The resistance could be related to the graphitization degree of carbon fibers with a turbostratic structure, which may be influenced by the carbonization temperature [36,37]. In addition, the densification of the ceramic composites may further compact the carbon fibers inside, which could contribute to the increased conductivity of the ceramic composites obtained at higher temperature. The as-prepared composite can be used as an electric heater to achieve electricity and heat conversion. All four composites showed similar curves of temperature vs. time (Figure 6b), where the temperature of the composites increased as the heating time was prolonged. For Composite-1350, the temperature increased quickly within the first minute, and reached 100 °C after 15 s and 200 °C after 90 s at 5 V (Figure 6b). Then, the heating rate decreased gradually and reached a stabilized temperature after 600 s (Figure 6b). It was also observed that the composite sintered at a higher temperature showed better joule heating performance. The highest temperature achieved by Composite-1250 was 241 °C, which increased to 292 °C for Composite-1350. Higher voltage led to a faster temperature rising rate and higher stabilized temperature. Figure 6c shows that the temperature of Composite-1350 increased from 57 °C to 292 °C when the voltage increased from 2 V to 5 V. A good linear correlation (R^2 = 0.99979) between the temperature and U^2 was observed in Figure 6d.

The heat stability of the ceramic composite was investigated by performing several power on/power off cycles. In each cycle, after the ceramic composite reached the stabilized temperature, the power was turned off until the ceramic composite cooled down to room temperature. As shown in Figure 7a, the ceramic composite reached 56 °C at 2 V and then reached 292 °C at 5 V. After three cycles, the temperature rise/drop curve and stabilized temperature was maintained at 5 V, which indicates that the composite had good heating stability performance. The heat distribution of the composites are shown in Figure 7b. When the current passed through the carbon fibers, the composite surface above the carbon fibers showed a higher temperature than the edges. The surface temperature increased with an increase in the power-on time. When the power was turned off, the heat spread from the center to the edges. Finally, during the cooling down process, the heat evenly distributed on the surface of the composite at 26 °C. The ceramic composite was also used as a heating element to heat 50 mL of water under 12 V (Figure 7c). The water in the beaker boiled after 15 minutes. The ceramic composite showed a good joule heating performance, which could be used as a water heater.

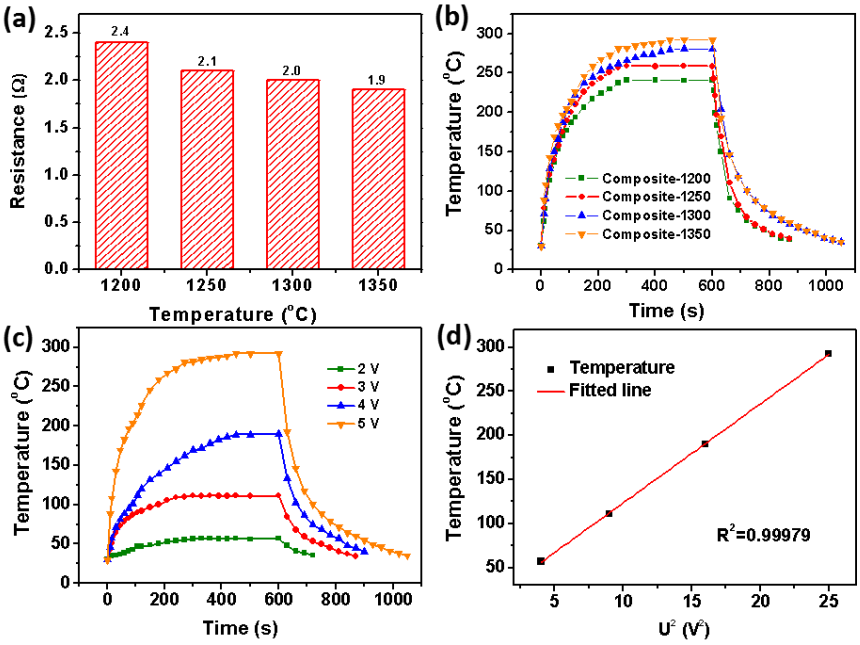


Figure 6. Electro-thermal performance of the composites. (**a**) Resistance of the specimens; (**b**) temperature changes of the specimens at 5 V; (**c**) temperature changes of Composite-1350 from 2 V to 5 V; (**d**) temperature-U^2 relationship for Composite-1350.

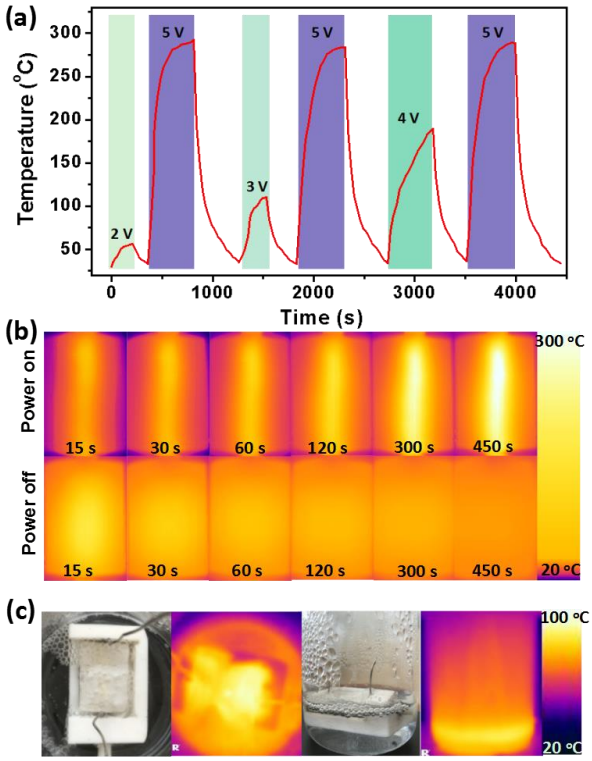


Figure 7. Electro-thermal performance of Composite-1350. (**a**) Cyclic performance of joule heating. (**b**) Infrared thermal images at 5 V and (**c**) ceramic composite was put into a beaker with 50 mL water under 12 V.

4. Conclusions

This work investigated the feasibility of using stabilized PAN in the green body of the ceramic to obtain carbon fiber/ceramic composites by a single firing. The pre-oxidated PAN could be carbonized

in the ceramic matrix with a firing temperature between 1200 °C and 1350 °C. Increasing the sintering temperature from 1200 °C to 1350 °C resulted in increased flexural strength of the composites, which was 28.88 ± 2.52 MPa for the composite fired at 1350 °C. It was also observed that increasing the firing temperature reduced the resistance of obtained carbon fibers, therefore leading to an increase of the highest temperature of the carbon fiber/ceramic composite during the electric heating process. The obtained carbon fiber/ceramic composites exhibited great electro-thermal performance, which reached more than 100 °C after 15 s and 200 °C after 90 s at 5 V for Composite-1350. This novel carbon fiber/ceramic produced from the one-step firing method has good potential to be used as an indoor electric heater, defogger device, kettle, and other heating element.

Author Contributions: Conceptualization, J.W.; Formal analysis, X.L. and Q.L.; Investigation, D.L., W.C., and X.D.; Methodology, D.L. and B.T.; Supervision, J.W. and X.W.; Writing – original draft, D.L., B.T., and J.W.; Writing – review & editing, X.W.

Funding: This work was funded by the Wuhan Textile University (WTU) and Deakin University through the Deakin-WTU Joint PhD Program. The research was also supported by Jiangsu BOHN Environmental Engineering & Complete Equipment Co., Ltd.

Conflicts of Interest: The authors declare no conflicts of interest.

References

1. Zhang, M.; Wang, C.; Liang, X.; Yin, Z.; Xia, K.; Wang, H.; Jian, M.; Zhang, Y. Weft-knitted fabric for a highly stretchable and low-voltage wearable heater. *Adv. Electron. Mater.* **2017**, *3*, 1700193. [CrossRef]
2. Jang, H.-S.; Jeon, S.K.; Nahm, S.H. The manufacture of a transparent film heater by spinning multi-walled carbon nanotubes. *Carbon* **2011**, *49*, 111–116. [CrossRef]
3. Ji, S.; He, W.; Wang, K.; Ran, Y.; Ye, C. Thermal response of transparent silver nanowire/pedot: Pss film heaters. *Small* **2014**, *10*, 4951–4960. [CrossRef] [PubMed]
4. Zhang, L.; Baima, M.; Andrew, T.L. Transforming commercial textiles and threads into sewable and weavable electric heaters. *ACS Appl. Mater. Interfaces* **2017**, *9*, 32299–32307. [CrossRef]
5. Lu, P.; Cheng, F.; Ou, Y.; Lin, M.; Su, L.; Chen, S.; Yao, X.; Liu, D. A flexible and transparent thin film heater based on a carbon fiber/heat-resistant cellulose composite. *Compos. Sci. Technol.* **2017**, *153*, 1–6. [CrossRef]
6. Cheng, C.; Ke, K.-C.; Yang, S.-Y. Application of graphene–polymer composite heaters in gas-assisted micro hot embossing. *RSC Adv.* **2017**, *7*, 6336–6344. [CrossRef]
7. Javed, H.; Islam, M.; Mahmood, N.; Achour, A.; Hameed, A.; Khatri, N. Catalytic growth of multi-walled carbon nanotubes using nife2o4 nanoparticles and incorporation into epoxy matrix for enhanced mechanical properties. *J. Ploym. Eng.* **2016**, *36*, 53–64. [CrossRef]
8. Cheng, Y.; Zhang, H.; Wang, R.; Wang, X.; Zhai, H.; Wang, T.; Jin, Q.; Sun, J. Highly stretchable and conductive copper nanowire based fibers with hierarchical structure for wearable heaters. *ACS Appl. Mater. Interfaces* **2016**, *8*, 32925–32933. [CrossRef]
9. Pampuch, R. *Ceramic Materials: An Introduction to Their Properties*; Elsevier Science & Technology: Amsterdam, The Netherlands, 1976.
10. Dana, K.; Das, S.; Das, S.K. Effect of substitution of fly ash for quartz in triaxial kaolin–quartz–feldspar system. *J. Eur. Ceram. Soc.* **2004**, *24*, 3169–3175. [CrossRef]
11. Harabi, A.; Guerfa, F.; Harabi, E.; Benhassine, M.-T.; Foughali, L.; Zaiou, S. Preparation and characterization of new dental porcelains, using k-feldspar and quartz raw materials. Effect of b 2 o 3 additions on sintering and mechanical properties. *Mater. Sci. Eng. C Mater. Biol. Appl.* **2016**, *65*, 33–42. [CrossRef]
12. Schneider, H.; Schreuer, J.; Hildmann, B. Structure and properties of mullite—A review. *J. Eur. Ceram. Soc.* **2008**, *28*, 329–344. [CrossRef]
13. Wu, J.; Jones, F.; James, P. Continuous fibre reinforced mullite matrix composites by sol–gel processing: Part i fabrication and microstructures. *J. Mater. Sci.* **1997**, *32*, 3361–3368. [CrossRef]
14. Wu, J.; Jones, F.; James, P. Continuous fiber reinforced mullite matrix composites by sol–gel processing: Part ii properties and fracture behaviour. *J. Mater. Sci.* **1997**, *32*, 3629–3635. [CrossRef]
15. Chen, L.; Yin, X.; Fan, X.; Chen, M.; Ma, X.; Cheng, L.; Zhang, L. Mechanical and electromagnetic shielding properties of carbon fiber reinforced silicon carbide matrix composites. *Carbon* **2015**, *95*, 10–19. [CrossRef]

16. Ehrburger, P.; Donnet, J.; Ubbelohde, A.; Johnson, J.; Richardson, M.; Scott, R. Interface in composite materials. *Philos. Trans. R. Soc. A* **1980**, *294*, 495–505. [CrossRef]
17. Liu, H.; Ma, Q.; Liu, W. Mechanical and oxidation resistance properties of 3d carbon fiber-reinforced mullite matrix composites prepared by sol–gel process. *Ceram. Int.* **2014**, *40*, 7203–7212. [CrossRef]
18. Ebadzadeh, T. Formation of mullite from precursor powders: Sintering, microstructure and mechanical properties. *Mater. Sci. Eng. A Struct. Mater. Prop.* **2003**, *355*, 56–61. [CrossRef]
19. Chawla, K. Interface engineering in mullite fiber/mullite matrix composites. *J. Eur. Ceram. Soc.* **2008**, *28*, 447–453. [CrossRef]
20. Dumanlı, A.G.; Windle, A.H. Carbon fibres from cellulosic precursors: A review. *J. Mater. Sci.* **2012**, *47*, 4236–4250. [CrossRef]
21. Yusof, N.; Ismail, A. Post spinning and pyrolysis processes of polyacrylonitrile (pan)-based carbon fiber and activated carbon fiber: A review. *J. Anal. Appl. Pyrol.* **2012**, *93*, 1–13. [CrossRef]
22. Iqbal, Y.; Lee, W.E. Microstructural evolution in triaxial porcelain. *J. Am. Ceram. Soc.* **2000**, *83*, 3121–3127. [CrossRef]
23. Ece, O.I.; Nakagawa, Z.-E. Bending strength of porcelains. *Ceram. Int.* **2002**, *28*, 131–140. [CrossRef]
24. Martín-Márquez, J.; Rincón, J.M.; Romero, M. Effect of firing temperature on sintering of porcelain stoneware tiles. *Ceram. Int.* **2008**, *34*, 1867–1873. [CrossRef]
25. Martín-Márquez, J.; Rincón, J.M.; Romero, M. Mullite development on firing in porcelain stoneware bodies. *J. Eur. Ceram. Soc.* **2010**, *30*, 1599–1607. [CrossRef]
26. Dasgupta, S.; Ganguli, D.; Roy, S.K.; Kumar, S. *Chemical Analysis of Ceramic and Allied Materials*; Indian Institute of Ceramics: Andhra Pradesh, Indian, 1985.
27. *BS EN ISO 10545-3:2018 Ceramic Tiles. Determination of Water Absorption, Apparent Porosity, Apparent Relative Density and Bulk Density*; ISO: Geneva, Switzerland, 2018. [CrossRef]
28. Lerdprom, W.; Grasso, S.; Jayaseelan, D.D.; Reece, M.J.; Lee, W.E. Densification behaviour and physico-mechanical properties of porcelains prepared using spark plasma sintering. *Adv. Appl. Ceram.* **2017**, *116*, 307–315. [CrossRef]
29. Chen, C.; Lan, G.; Tuan, W. Microstructural evolution of mullite during the sintering of kaolin powder compacts. *Ceram. Int.* **2000**, *26*, 715–720. [CrossRef]
30. Rodríguez, E.A.; Niño, C.J.; Contreras, J.E.; Vázquez-Rodríguez, F.; Perales, J.L.; Aguilar-Martínez, J.; Puente-Ornelas, R.; Banda, M.L. Influence of incorporation of fired porcelain scrap as partial replacement of quartz on properties of an electrical porcelain. *J. Clean. Prod.* **2019**. [CrossRef]
31. Štubňa, I.; Chmelík, F.; Trník, A.; Šín, P. Acoustic emission study of quartz porcelain during heating up to 1150 °C. *Ceram. Int.* **2012**, *38*, 6919–6922. [CrossRef]
32. Malard, L.; Pimenta, M.; Dresselhaus, G.; Dresselhaus, M. Raman spectroscopy in graphene. *Phys. Rep.* **2009**, *473*, 51–87. [CrossRef]
33. Hambach, M.; Möller, H.; Neumann, T.; Volkmer, D. Carbon fibre reinforced cement-based composites as smart floor heating materials. *Compos. Part B Eng.* **2016**, *90*, 465–470. [CrossRef]
34. Karacan, I.; Erzurumluoğlu, L. The effect of carbonization temperature on the structure and properties of carbon fibers prepared from poly (m-phenylene isophthalamide) precursor. *Fibers Polym.* **2015**, *16*, 1629–1645. [CrossRef]
35. Kakali, G.; Perraki, T.; Tsivilis, S.; Badogiannis, E. Thermal treatment of kaolin: The effect of mineralogy on the pozzolanic activity. *Appl. Clay Sci.* **2001**, *20*, 73–80. [CrossRef]
36. Aliev, A.E.; Perananthan, S.; Ferraris, J.P. Carbonized electrospun nanofiber sheets for thermophones. *ACS Appl. Mater. Interfaces* **2016**, *8*, 31192–31201. [CrossRef] [PubMed]
37. Kwon, J.H.; Park, S.B.; Ayrilmis, N.; Oh, S.W.; Kim, N.H. Effect of carbonization temperature on electrical resistivity and physical properties of wood and wood-based composites. *Compos. Part B Eng.* **2013**, *46*, 102–107. [CrossRef]



© 2019 by the authors. Licensee MDPI, Basel, Switzerland. This article is an open access article distributed under the terms and conditions of the Creative Commons Attribution (CC BY) license (http://creativecommons.org/licenses/by/4.0/).